

# Power Spectrum Analysis of the Stromlo-APM Redshift Survey

H. Tadros<sup>\*</sup> and G. Efstathiou

*Department of Physics, University of Oxford, Keble Road, Oxford, OX1 3RH. UK.*

11 September 2018

## ABSTRACT

We test estimators of the galaxy power spectrum  $P(k)$  against simulated galaxy catalogues constructed from N-body simulations and we derive formulae to correct for biases. These estimators are then applied to compute the power spectrum of galaxies in the Stromlo-APM redshift survey. We test whether the amplitude of  $P(k)$  depends on galaxy luminosity, but find no significant luminosity dependence except at absolute magnitudes brighter than  $M_{b_J} = -20.3$ , ( $H_0 = 100\text{km s}^{-1}$ ) where there is some evidence for a rise in the amplitude of  $P(k)$ . By comparing the redshift space power spectrum of the Stromlo-APM survey with the real space power spectrum determined from the parent APM Galaxy Survey, we attempt to measure the distortion in the shape of  $P(k)$  caused by galaxy peculiar motions. We find some evidence for an effect, but the errors are large and do not exclude a value of  $\beta = \Omega^{0.6}/b = 1$ , where  $\Omega$  is the cosmological density parameter and  $b$  is the linear biasing parameter relating galaxy fluctuations to those in the mass,  $(\delta\rho/\rho)_{gal} = b(\delta\rho/\rho)_m$ . The shape of the Stromlo-APM power spectrum is consistent with that determined from the CfA-2 survey, but has a slightly higher amplitude by a factor of about 1.4 than the power spectrum of IRAS galaxies.

**Key words:** Galaxy clustering; Cosmology; Large-scale structure

## 1 INTRODUCTION

The Stromlo-APM redshift survey is a 1 in 20 sparsely sampled subset of 1787 galaxies selected from the APM Galaxy survey (Maddox *et al.* 1990a) to a magnitude limit of  $b_J = 17.15$ . The survey has been used in several investigations of the large-scale clustering of galaxies: Loveday *et al.* (1992a) have investigated galaxy counts in nearly cubical cells with sizes in the range  $5 h^{-1}\text{Mpc} - 60 h^{-1}\text{Mpc}$ ; Loveday *et al.* (1995a) have computed the two-point galaxy correlation function of the Stromlo-APM survey and Loveday *et al.* (1995b) have investigated anisotropies in the two-point correlation function caused by redshift-space distortions (see Kaiser 1987). In this paper, we present an analysis of the power spectrum,  $P(k)$ , of galaxies in the Stromlo-APM survey. The power spectrum of the galaxy distribution has been estimated from a number of other surveys (see Efstathiou 1996 for a review). Power spectra for optically selected samples have been computed by *e.g.* Baumgart and Fry (1991), Vogeley *et al.* (1992), Park *et al.* (1994) and Baugh and Efstathiou (1993, 1994). Power spectra for various IRAS red-

shift surveys have been computed by Fisher *et al.* (1993), Feldman, Kaiser and Peacock (1994, hereafter FKP) and Tadros and Efstathiou (1995).

The layout of this paper is as follows. The Stromlo-APM redshift survey is described in Section 2. In Sections 3 and 4, we discuss estimators of the power spectrum and their biases and test our techniques against simulated Stromlo-APM redshift surveys constructed from large N-body simulations. In Section 5 we present estimates of the power spectrum for volume limited and flux limited samples selected from the Stromlo-APM survey and we investigate the sensitivity of the results to the volume limit and the weights assigned to the galaxies. A number of authors have claimed that luminous galaxies are more strongly clustered than less luminous galaxies (*e.g.* Hamilton 1988, Santiago and da Costa 1990, Iovino *et al.* 1993, Park *et al.* 1994). We investigate the dependence of clustering strength with luminosity in Section 5. In Section 6 we investigate the distortion of the power spectrum measured in redshift space caused by galaxy peculiar motions and we attempt to measure the effect by comparing the redshift-space estimates of  $P(k)$  from the Stromlo-APM survey with real-space estimates of  $P(k)$  inferred from the parent APM catalogue (see Baugh and Efstathiou 1993). We present our main conclusions in Sec-

<sup>\*</sup> Current address: Astronomy Centre, University of Sussex, Falmer, Brighton, UK

tion 7 and compare our estimates of  $P(k)$  with those for the CfA-2 survey and IRAS surveys and with the predictions of various cold dark matter models.

## 2 DATA SET

The Stromlo-APM redshift survey is described in detail by Loveday *et al.* (1992a). The survey covers an area approximately defined by the equatorial coordinates  $21^h \lesssim \alpha \lesssim 5^h$ ,  $-72.5^\circ \lesssim \delta \lesssim -17.5^\circ$ . In the analysis described below, we analyse flux limited and volume limited samples. The volume limited samples are constructed by removing all galaxies with redshifts  $z > z_{max}$  and absolute magnitudes  $M > M_{crit}$ , where

$$M_{crit} = m_{lim} - 25 - 5 \log(d_L(z_{max})) - kz_{max}, \quad (1)$$

$m_{lim} = 17.15$  is the magnitude limit of the survey and  $d_L(z_{max})$  is the luminosity distance at redshift  $z_{max}$ . Throughout this paper, we assume a spatially flat universe with  $\Omega = 1$ , thus

$$d_L(z) = \frac{2c}{H_0} \left[ 1 - \frac{1}{\sqrt{1+z}} \right] (1+z). \quad (2)$$

The median redshift of the Stromlo-APM survey is  $z = 0.05$ , hence the results presented below are insensitive to the assumed cosmological model. We adopt a  $k$  correction of  $3z$  in equation (1) which is appropriate for the median morphological type in the Stromlo-APM survey in the  $b_J$  passband (Efstathiou, Ellis and Peterson 1988).

There are some advantages in estimating power spectra from volume limited rather than flux limited samples. Firstly, every galaxy in a volume limited sample carries equal weight, whereas weighting factors that are a function of the power spectrum  $P(k)$  are required to determine a minimum variance estimate of  $P(k)$  from a flux limited sample if the underlying density field is assumed to be Gaussian (see FKP and Section 3). Secondly, the analysis of flux limited samples requires a model for the mean galaxy density  $\bar{n}(r)$  as a function of radial distance. Thirdly, by estimating power spectra of progressively larger volume limited samples it is possible, given a large enough sample, to test whether the clustering amplitude is a function of luminosity. These points will be discussed in further detail in Section 4.

The solid line in Figure 1 shows the number of galaxies in volume limited subsamples of the Stromlo-APM survey as a function of the limiting redshift  $z_{max}$ . The total number of galaxies peaks at  $z_{max} = 0.06$ , corresponding to an absolute magnitude limit of  $-19.34^\dagger$ . For most of the analysis in this paper we adopt a volume limit of  $z_{max} = 0.06$  (coordinate distance of  $x_{max} = 172 h^{-1} \text{Mpc}$ ) containing 469 galaxies. The dashed curve in Figure 1 shows the number of galaxies predicted by integrating over the galaxy luminosity function:

$$N(z_{max}) = \phi_* V(z_{max}) \int_{L_{min}(z_{max})}^{\infty} \left( \frac{L}{L_*} \right)^\alpha e\left(-\frac{L}{L_*}\right) d\left(\frac{L}{L_*}\right) \quad (3)$$

<sup>†</sup> Throughout this paper, we write the Hubble constant as  $H_0 = 100h \text{ km s}^{-1} \text{ Mpc}^{-1}$  and quote absolute magnitudes assuming  $h = 1$  unless otherwise stated.

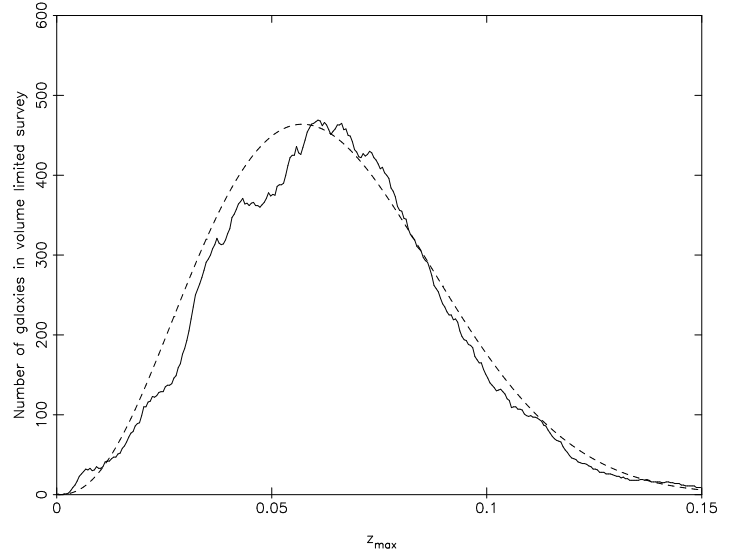


**Figure 1.** The solid line shows the number of galaxies in volume limited subsamples of the Stromlo-APM survey as a function of limiting redshift  $z_{max}$ . The dashed curve shows the expected distribution derived by integrating the luminosity function from Loveday *et al.* (1992a) using the Schechter function parameters given in the text.

where  $V(z_{max})$  is the comoving volume of the survey to redshift  $z_{max}$ , and  $L_{min}$  is the luminosity of a galaxy with absolute magnitude  $M_{crit}$  (equation 1). We have used the luminosity function parameters from Loveday *et al.* (1992b)  $\phi_* = 1.12 \times 10^{-2} h^3 \text{Mpc}^{-3}$ ,  $\alpha = -1.11$  and  $M_* = -19.73$ ; these are the best fitting Schechter (1976) function parameters for galaxies with absolute magnitudes in the range  $-22 < M < -15$ , uncorrected for magnitude errors.

## 3 MEASUREMENT OF THE POWER SPECTRUM

In this Section we establish our notation and describe our estimator of  $P(k)$ . We imagine that the Universe is divided into infinitesimal cells of volume  $\delta V$  containing  $n_i$  galaxies such that the  $n_i$  are either 0 or 1. The mean and variance of  $n_i$  are therefore,

$$\langle n_i \rangle = \bar{n} \delta V \quad (4)$$

$$\langle n_i^2 \rangle = \langle n_i \rangle \quad (5)$$

The observed galaxy count  $n_o(\mathbf{x}_i)$  at point  $\mathbf{x}_i$  is related to the real galaxy count  $n_i$  by

$$n_o(\mathbf{x}_i) = n_i W(\mathbf{x}_i), \quad (6)$$

where  $W(\mathbf{x}_i)$  defines the window function of the survey. In general, the window function depends on the radial distribution of galaxies in the survey, the survey boundaries on the celestial sphere, and the weights applied to each galaxy. In this section, we assume that we are analysing a volume limited sample in which each galaxy is assigned equal weight. In this case, the window function  $W(\mathbf{x})$  is equal to unity or zero according to whether a particular patch of the universe is included or excluded from the survey. It is straightforward to generalize the equations in this Section to more complex

window functions and to include radially dependent galaxy weights (see FKP).

For the Stromlo-APM survey, the window function is defined by an angular mask consisting of the APM Galaxy Survey boundaries together with rectangular holes around regions on the plates where there are bright stars, satellite trails, globular clusters, step-wedges *etc* (see Plate 2 of Maddox *et al.* 1990b). We estimate the Fourier transform of the window function

$$\hat{W}(\mathbf{k}) = \frac{1}{V} \int W(\mathbf{x}) e^{i\mathbf{k}\cdot\mathbf{x}} d^3\mathbf{x} \quad (7)$$

by generating a large number random points with mean density  $\bar{n}_R$  within the survey volume and computing

$$\hat{W}_e(\mathbf{k}) = \frac{1}{\bar{n}_R V} \sum_i e^{i\mathbf{k}\cdot\mathbf{x}_i}, \quad (8)$$

where the sum extends over all random points located at positions  $\mathbf{x}_i$ . The volume  $V$  is a normalizing volume which encloses the survey.

We compute the Fourier transform of the observed density field

$$\hat{n}_o(\mathbf{k}) = \frac{1}{V} \sum_i n_i e^{i\mathbf{k}\cdot\mathbf{x}_i}, \quad (9)$$

and we define a variable with zero mean

$$\Delta(\mathbf{k}) = \hat{n}_o(\mathbf{k}) - \bar{n}\hat{W}(\mathbf{k}), \quad (10)$$

where  $\bar{n}$  is the mean galaxy density. The variance of  $\Delta(\mathbf{k})$  is related to the power spectrum  $P(k)$  of the galaxy distribution according to

$$\langle |\Delta(\mathbf{k})|^2 \rangle = \frac{\bar{n}}{V} \sum_{\mathbf{k}'} |\hat{W}(\mathbf{k}')|^2 + \frac{\bar{n}^2}{V} \sum_{\mathbf{k}'} |\hat{W}(\mathbf{k}-\mathbf{k}')|^2 P(\mathbf{k}'). \quad (11)$$

Figure 2 shows the window function of the Stromlo-APM survey region volume limited at  $z = 0.06$ . This figure shows that the window function is sharply peaked in  $\mathbf{k}$ -space, falling off approximately as  $k^{-4}$ . We have computed the sum in equation (8) by Fast Fourier transforming the random density field within a cubical volume of side  $840 h^{-1} \text{Mpc}$ . We also plot the components of  $|W(\mathbf{k})|^2$  along the principal axes of the cube, showing that the window function is anisotropic and is narrower in the  $x$ -direction, which is aligned along the radial direction of the centre of the survey.

Since the window function is sharply peaked in  $\mathbf{k}$ -space, it is a good approximation to remove  $P(\mathbf{k}')$  from the summation in equation (11), thus our estimate of  $P(\mathbf{k})$  is

$$P_e(\mathbf{k}) = \frac{\frac{V^2}{N_G^2} |\Delta(\mathbf{k})|^2 - \frac{1}{N_G} - \frac{1}{N_R}}{\frac{V}{V_s} \sum_{\mathbf{k}'} |W_e(\mathbf{k}')|^2}, \quad (12)$$

where  $N_G$  and  $N_R$  are the total number of galaxy and random points within the survey volume  $V_s$ ,

$$V_s = \int W(\mathbf{x}) d^3\mathbf{x}. \quad (13)$$

The negative terms in equation (12) correct for Poisson shot noise in the galaxy and random number distributions. Notice that in equation (12) we have assumed that the mean galaxy density is equal to  $N_G/V_s$ . The estimate  $P_e$  will therefore be biased low because the estimate of the mean galaxy density

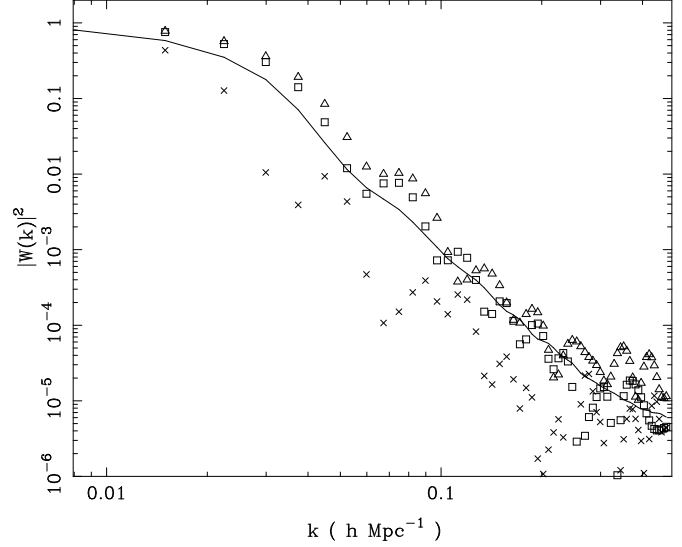


**Figure 2.** The Fourier transform of the Stromlo-APM survey volume limited at  $z = 0.06$ . The solid line shows the window function averaged in radial shells in  $\mathbf{k}$ -space while the crosses, squares and triangles show  $|W(k_x, 0, 0)|^2$ ,  $|W(0, k_y, 0)|^2$ , and  $|W(0, 0, k_z)|^2$  components respectively. The x-axis is aligned approximately along the radial direction pointing to the centre of the survey on the celestial sphere. We have normalized the curves so that they are equal to unity at  $k = 0$ .

is affected by galaxy clustering. An expression for this bias is derived in Appendix A.

We estimate the sampling errors on the power spectrum in two different ways. The first method is based on the error analysis of FKP who assume that the galaxy density field is a Gaussian point process. In the case of a volume limited survey, equation (2.4.6) of FKP for the error on the point with wave vector  $k$  is, in our notation,

$$\sigma_P(k) = \frac{V_s}{N_G} \frac{(1 + \frac{N_G}{N_R} + \bar{n}P(k))}{\sum_{\mathbf{k}'} |\hat{W}(\mathbf{k}')|^2} \times \left( \frac{1}{N_{sum}} \sum_{\mathbf{k}'} \sum_{\mathbf{k}''} |\hat{W}(\mathbf{k}' - \mathbf{k}'')|^2 \right)^{\frac{1}{2}} \quad (14)$$

In equation (14),  $\mathbf{k}'$  and  $\mathbf{k}''$  are constrained to lie in the same shell with modulus  $k$  and  $N_{sum}$  is the total number of terms in the double summation.

The second method is based on the variance of  $P(k)$  derived from mock Stromlo-APM surveys constructed from N-body simulations. The mock surveys, and a comparison with the FKP errors derived from equation (14) are described in Section 4.2. This is a useful test because equation (14) assumes Gaussian statistics, whereas the true galaxy density field is non-Gaussian at least on scales  $\lesssim 5 h^{-1} \text{Mpc}$  where the *rms* fluctuations exceed unity. By comparing the errors from mock catalogues which are non-Gaussian on small scales, we can check the accuracy of equation (14) over the full range of wavenumbers presented in this paper.

In the above analysis, we have assumed that we are analysing volume limited samples and assigning an equal weight to each galaxy. The analysis of a flux limited sample is more complicated because the window function  $W(\mathbf{x})$  depends on radial distance, and because we must assign radi-

ally dependent weights to the galaxies to minimise the variance on  $P(k)$ . These points are discussed in detail by FKP and we follow their analysis in this paper. If the underlying density fluctuations are Gaussian, FKP show that the variance on the estimated  $P(k)$  is minimised if each galaxy is assigned a weight

$$w(r) = \frac{1}{1 + \bar{n}(r)P(k)}, \quad (15)$$

where  $\bar{n}(r)$  is the mean galaxy density as a function of radial distance  $r$ , which we compute from the luminosity function of the Stromlo-APM survey with the parameters given in Section 2. From equation (15), we see that the minimum variance weighting for each wavenumber  $k$ , depends on the true value of the power spectrum at wavenumber  $k$ . Rather than applying different weights at each wavenumber, we have estimated the power spectrum from the flux-limited survey for four values of  $P(k)$  in equation (15),  $P(k) = 4000, 8000, 16000$  and  $32000$  ( $h^{-1}\text{Mpc}$ )<sup>3</sup>, which span the range of interest at wavenumbers  $\lesssim 0.3h\text{Mpc}^{-1}$ . Our analysis of flux limited surveys follows that of FKP except that we compute  $\alpha$  (the ratio of the space densities in the real catalogue to that in the random catalogue, equation 2.1.3 of FKP) from the ratio of the sums

$$\sum_i \frac{1}{(1 + 4\pi\bar{n}(r_i)J_3)}, \quad (16)$$

instead of  $\alpha = N_G/N_R$ , where the summations are over all galaxies and random points. We have set  $4\pi J_3 = 10000(h^{-1}\text{Mpc})^3$  (see Tadros and Efstathiou 1995).

#### 4 TESTS OF THE ESTIMATORS USING N-BODY SIMULATIONS

In this Section, we investigate the accuracy with which we can recover the power spectrum from the Stromlo-APM survey using the methods described in the previous Section. There are three key aspects of the analysis that we wish to test: (i) the assumption that the convolution of the window function with the power spectrum in equation (11) can be replaced by a product as in equation (12); (ii) the bias in the estimate of  $P(k)$  caused by estimating the mean galaxy density from the survey itself (Appendix A); (iii) the accuracy of the FKP error estimates (equation 14). We test these points by analysing mock Stromlo-APM surveys constructed from N-body simulations.

##### 4.1 Numerical Simulations

The numerical simulations that we use here are described by Croft and Efstathiou (1994). They consist of three ensembles of 10 simulations each containing  $10^6$  particles within a periodic computational box of length  $\ell = 300 h^{-1}\text{Mpc}$ . The simulations were run with the particle-particle-particle-mesh (P<sup>3</sup>M) code described by Efstathiou *et al.* (1985). The simulations model gravitational clustering in a cold dark matter (CDM) dominated universe with scale invariant initial density fluctuations. The three ensembles are as follows: the standard CDM model (Davis *et al.* 1985), *i.e.* a spatially flat universe with  $\Omega_0 = 1$  and  $h = 0.5$  (SCDM); a spatially

flat low density CDM universe with  $\Omega_0 = 0.2$  and a cosmological constant  $\lambda = \frac{\Lambda}{3H_0^2} = (1 - \Omega_0) = 0.8$  (LCDM); a spatially flat mixed dark matter model in which CDM contributes  $\Omega_{CDM} = 0.6$ , baryons contribute  $\Omega_b = 0.1$  and massive neutrinos contribute  $\Omega_\nu = 0.3$ .

For the SCDM and LCDM simulation, the initial power spectrum is given by

$$P(k) \propto \frac{k}{\left[1 + \left(ak + (bk)^{\frac{3}{2}} + (ck)^2\right)^\nu\right]^{\frac{2}{\nu}}} \quad (17)$$

where  $\nu = 1.13$ ,  $a = \frac{6.4}{\Gamma} h^{-1}\text{Mpc}$ ,  $b = \frac{3.0}{\Gamma} h^{-1}\text{Mpc}$  and  $c = \frac{1.7}{\Gamma} h^{-1}\text{Mpc}$ . Equation (17) is a good approximation to the linear power spectrum of scale-invariant CDM models with low baryon density,  $\Omega_b \ll \Omega_0$  (Bond and Efstathiou 1984). The parameter  $\Gamma$  in equation (17) is equal to  $\Omega_0 h$ , thus  $\Gamma = 0.5$  for the SCDM ensemble and  $\Gamma = 0.2$  for the LCDM ensemble. The initial conditions for our MDM simulations are generated from the power spectrum given by equation 1 of Klypin *et al.* (1993). In the MDM models, we ignore the thermal motions of the neutrinos and so follow the evolution of a collisionless cold component with  $\Omega_0 = 1$ .

The final output times of the models are chosen to approximately match the microwave background anisotropies measured in the first year COBE maps (Smoot *et al.* 1992) ignoring any contribution from gravitational waves. Thus the *rms* mass fluctuations in spheres of radius  $8 h^{-1}\text{Mpc}$  are  $\sigma_8 = 1$  for the SCDM and LCDM ensembles and  $\sigma_8 = 0.67$  for the MDM ensemble. Normalizing the anisotropies measured from the combined first and second year COBE maps would increase these values of  $\sigma_8$  by  $\sim 20\text{--}30\%$ , but these small changes are unimportant for most of the discussion below.

##### 4.2 Mock Stromlo-APM Surveys

From the simulations described above we have constructed mock Stromlo-APM surveys. We assume that galaxies are distributed like the mass points in the simulations and make no attempt to introduce biasing. We apply the APM angular mask to the simulations and replicate the periodic box where necessary to generate distant points. We then generate fully sampled volume limited catalogues to  $z_{max} = 0.06$  that contain typically 100,000 mass points. We also generate volume limited samples containing on average 469 points by random sampling the mass points. These mock surveys thus have similar numbers of points as there are galaxies in the Stromlo-APM survey at this volume limit. Flux limited surveys are also generated by selecting mass points with the radial selection function of the Stromlo-APM survey (see Section 2).

Figure 3 shows three estimates of the power spectrum in real space measured for each ensemble. The solid lines show the mean of the power spectra determined from the full cubical N-body simulations. These are computed by Fast Fourier transforming the particle distribution on a  $128^3$  grid using the nearest grid point assignment scheme, as described by Efstathiou *et al.* (1985). The open squares show the power spectra derived from equation (12) for the fully sampled mock Stromlo-APM surveys volume limited at  $z_{max} = 0.06$ . The symbols show the mean value of  $P(k)$  from the ten mem-

bers of each ensemble and the error bars show the standard deviation on the mean derived from the scatter in the  $P(k)$  estimates. The open squares are in very good agreement with the power spectra of the full simulations at wavenumbers  $k \gtrsim 0.04h\text{Mpc}^{-1}$ , showing that replacing the convolution over  $P(k)$  in equation (11) by a product is an excellent approximation. At smaller wavenumbers, the power spectrum is systematically underestimated. This is caused by the bias associated with the mean density estimate described in Appendix A. The dashed curves in Figure 3 show the linear theory power spectra for each model including an approximate correction for the bias derived from equation (A4.2) of Appendix A. These curves are in excellent agreement with the data points, showing that the bias can be removed if the form of the power spectrum is known. The filled triangles show the power spectra for volume limited ( $z_{max} = 0.06$ ) realizations of the sparse sampled Stromlo-APM survey. As described above, these simulations have approximately the same number of objects as in the real catalogue and accurately model the window function of the real survey. Because the number of points in each realization is small (and hence the errors on  $P(k)$  are large), we have plotted the averages over 30 realizations from each ensemble. The results are very similar to those from the fully sampled Stromlo-APM simulations, except that the bias associated with the mean density estimate is larger, as expected from equation (A4.2) of Appendix A (shown by the dashed lines passing through the points).

In Figure 4 we analyse flux limited sparse-sampled Stromlo-APM surveys for the SCDM and LCDM ensembles using the techniques of FKP. Each panel shows the power spectra averaged over 10 realizations for four values of  $P(k)$  in the weighting scheme of equation (15) as indicated in each panel. The results are qualitatively similar to those of Figure 3 and show that the FKP estimator provides an unbiased estimate of  $P(k)$  at wavenumbers  $k \gtrsim 0.04h\text{Mpc}^{-1}$ . Furthermore, Figure 4 shows that the estimates of  $P(k)$  and the errors on  $P(k)$  are relatively insensitive to the weighting scheme. This is as expected since a minimum variance estimator should not be sensitive to small departures from the minimum variance weighting scheme. The errors on  $P(k)$  at wavenumbers  $k \gtrsim 0.1h\text{Mpc}^{-1}$  are noticeably larger if we adopt a constant value of  $P(k) \geq 16000(h^{-3}\text{Mpc})^3$  in the weighting scheme (15), but it is clear that this is an overestimate of the amplitude of the power spectrum at these wavenumbers.

We have also investigated the accuracy of the error estimates derived from equation (14) and its generalization to flux limited samples by comparing with the dispersion in the  $P(k)$  estimates from our mock surveys. Equation (14) provides an accurate estimate of the errors for wavenumbers  $k \lesssim 0.1h\text{Mpc}^{-1}$ , but tends to underestimate the errors by a factor of  $\sim 2$  at larger wavenumbers.

In summary, the results of this Section show that our methods provide nearly unbiased estimates of the power spectrum at wavenumbers  $k \gtrsim 0.04h\text{Mpc}^{-1}$ . At smaller wavenumbers, the estimates are biased low because we determine the mean galaxy density from the sample itself. The power spectra derived from flux limited samples are insensitive to the weighting scheme, provided we adopt a reasonable value of  $P(k)$  in equation (15).

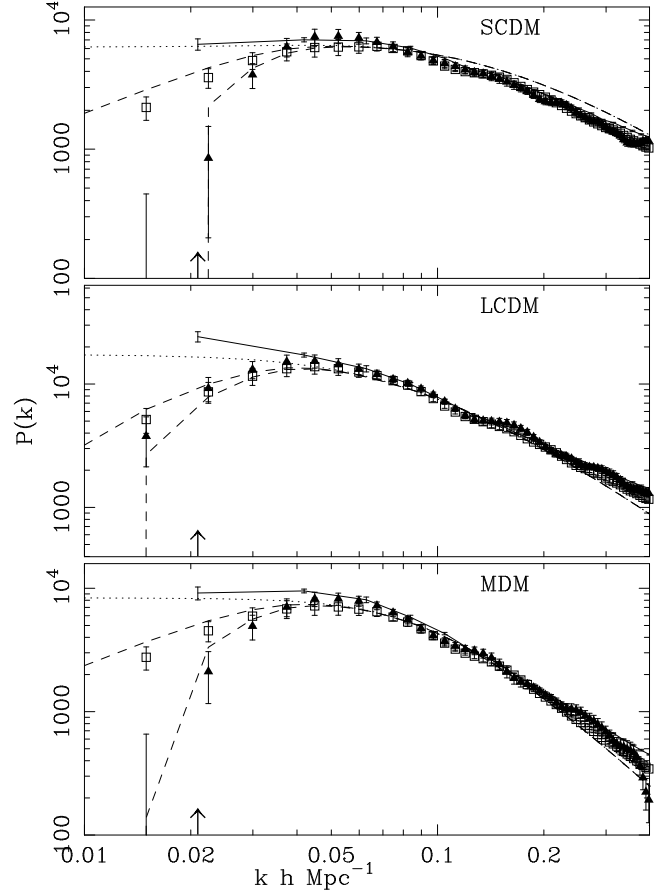


**Figure 3.** Estimates of the power spectra in real space for the three ensembles of N-body simulations described in the text. The solid lines show the average of the power spectra derived from the full cubical volume of the simulations. The open squares show the average of  $P(k)$  derived from equation (12) applied to 10 fully sampled realizations of the Stromlo-APM survey, volume limited at  $z_{max} = 0.06$ . The filled triangles show the average of  $P(k)$  over 30 realizations of the sparse-sampled Stromlo -APM survey volume limited at  $z_{max} = 0.06$ . The error bars in each case show the standard deviation of the mean. The dashed lines are derived from equation (A4.2) of Appendix A, assuming the linear theory form of the power spectrum for each ensemble and illustrate how the mock surveys are affected by the bias associated with the estimate of the mean galaxy density. The dotted lines show the convolution of the linear power spectrum (equation 17) with the window function for the Stromlo-APM survey. The arrows show the smallest wavenumber represented in the simulations,  $k = 2\pi/\ell_b$ , where  $\ell_b = 300 h^{-1}\text{Mpc}$  is the computational box length.

## 5 THE POWER SPECTRUM OF THE STROMLO-APM SURVEY

### 5.1 Comparison of results from volume limited and flux limited samples

In Figure 5 we show the power spectra for three volume limited subsets of the Stromlo-APM survey, together with  $1\sigma$  errors derived from the FKP formula (equation 14). The power spectra are consistent with each other, with no obvious dependence on the volume limit. The results are quali-

tatively similar to those of the simulations plotted in Figure 3. The power spectrum of the real survey has an approximately power law behaviour  $P(k) \propto k^{-1.7}$  at wavenumbers  $k \gtrsim 0.05h\text{Mpc}^{-1}$ , flattens off and declines at smaller wavenumbers. The decline is almost certainly caused by the bias discussed in Appendix A and so is not a real feature of the galaxy distribution. The Stromlo-APM survey contains little information at wavenumbers  $k \lesssim 0.05h\text{Mpc}^{-1}$ , since these scales are comparable to or greater than the size of the survey.

Figure 6 shows the flux limited power spectrum from the Stromlo-APM survey for four values of  $P(k)$  in the weighting function of equation (15). As in our analysis of the flux limited mock Stromlo-APM simulations (Figure 4) we see that the power spectra in Figure 6 are insensitive to the weighting scheme. The power spectra in Figures 5 and 6 peak at a maximum value of  $\sim 30000(h^{-3}\text{Mpc})^3$  at a wavenumber of  $\sim 0.05h\text{Mpc}^{-1}$  and decline to a value of  $\sim 4000(h^{-3}\text{Mpc})^3$  at wavenumbers  $\sim 0.15h\text{Mpc}^{-1}$ . Thus, over most of the wavenumber range plotted in Figure 6, a value of  $P(k) \sim 10^4(h^{-3}\text{Mpc})^3$  in equation (15) should result in an estimate of  $P(k)$  that is close to the minimum variance estimate. In the remainder of this paper, unless otherwise stated, we will use the flux limited power spectrum with  $P(k)$  set to  $8000(h^{-3}\text{Mpc})^3$  in equation (15).

In Figure 7, we compare the volume limited power spectrum estimate for  $z_{max} = 0.06$  with the flux limited estimate derived with  $P(k) = 8000(h^{-3}\text{Mpc})^3$  in equation (15). The estimates are consistent with each other within the  $1\sigma$  error bars. This figure, and the results shown in figures 4 to 6, show that the power spectrum estimates from the Stromlo-APM survey are robust. In summary, we find no obvious differences between the power spectra of the volume limited samples plotted in figure 5, or between the power spectra measured from flux limited samples with different weighting functions. This places some constraints on variations of the power spectrum as a function of galaxy luminosity which we discuss in further detail in the next subsection.

## 5.2 Variations of the clustering strength with galaxy luminosity

As mentioned in the introduction, several groups have claimed to find various correlations between the strength of the clustering pattern and galaxy luminosity. In this section we investigate this possibility by comparing the power spectrum measured from volume limited subsamples of the Stromlo-APM data as a function of volume limit. We have already seen from Figure 5 that there is little evidence for any systematic dependence on the amplitude of  $P(k)$  with volume limit over the range  $z_{max} = 0.05\text{--}0.07$ , corresponding to cuts in absolute magnitude of  $M_{crit} = -18.91$  at  $z_{max} = 0.05$  and  $M_{crit} = -19.71$  at  $z_{max} = 0.07$  (equation 1). As we increase the volume limit beyond  $z_{max} = 0.07$ , the number of galaxies in the Stromlo-APM survey declines exponentially and hence the errors on  $P(k)$  become large. We have therefore averaged the power spectrum estimates over a range of wavenumbers to test for a linear bias in  $P(k)$  (*i.e.* a change in amplitude independent of wavenumber) as a function of volume limit. This has been done as follows: we have computed the power spectra of six volume limited samples with  $z_{max} = 0.04, 0.05, 0.06, 0.07, 0.08, 0.09$ . These

power spectra were averaged to produce a mean power spectrum  $P_{av}(k)$ . For each volume limit, we computed the ratio  $P(k)/P_{av}(k)$ , which we averaged over the wavenumber range  $0.052 < k < 0.14h\text{Mpc}^{-1}$  to produce an estimate of the relative bias factor  $b^2(M_{crit})$  for each volume limit. As can be seen from Figure 6, the error bars on  $P(k)$  depend weakly on wavenumber, hence it is reasonable to compute  $b^2(M_{crit})$  as an unweighted average over wavenumber. These bias factors are plotted against  $M_{crit}$  in Figure 8. If there were no dependence of the clustering strength with luminosity, we would expect the resulting bias factors to be close to unity for all values of  $M_{crit}$ . In fact, we find that the relative bias factor is close to unity for most of the magnitude range, but is lower than unity for the faintest magnitude cut at  $M_{crit} = -18.4$  and higher than unity for the brightest magnitude cut at  $M_{crit} = -20.3$ .

To assess the statistical significance of these result, we have computed linear bias factors in exactly the same way for each of the 30 mock Stromlo-APM surveys constructed from the LCDM ensemble. The results are plotted as the crosses in Figure 8 together with the standard deviation for a single Stromlo-APM survey. The results from the mock surveys are close to unity over the entire magnitude range, as expected since there is no luminosity dependence of the clustering pattern in the simulations. These results show that there is no firm evidence for any luminosity dependence of the amplitude of the power spectrum determined from the Stromlo-APM survey. At the faintest magnitude cut, 7 out of 30 simulated catalogues gave a relative bias factor lower than that measured for the real data. For the brightest magnitude cut, only 2 out of 30 simulations gave a relative bias factor larger than that determined from the Stromlo-APM survey. Thus, there is tentative evidence that the amplitude of the power-spectrum may increase at high luminosities. These results seem consistent with previous work. Loveday *et al.* (1995a) found some evidence that the spatial two-point correlation function for galaxies in the Stromlo-APM survey in the magnitude range  $-19 < M < -15$  has a lower amplitude than that measured for brighter galaxies. The results of Figure 8 suggest that this may be caused by sampling fluctuations rather than a real luminosity dependence of the clustering pattern. Park *et al.* (1994) have analyzed the power spectra of volume limited subsets of the CfA-2 redshift survey and find evidence that the amplitude of the power spectrum for galaxies brighter than  $M^*$  is about 40% higher than the amplitude measured for fainter galaxies. This is consistent with the results plotted in Figure 8 and suggests that the rise in the relative bias factor at  $M_{crit} < -20.3$  may be a real feature of the galaxy distribution. Evidently, larger redshift surveys are required to firmly establish whether this effect is real but the results of this section show that over most of the luminosity range, the power spectra measured from the Stromlo-APM survey are consistent with the null hypothesis that the clustering strength is independent of luminosity.

## 6 REDSHIFT-SPACE DISTORTIONS OF THE POWER SPECTRUM

Galaxy peculiar velocities cause a distortion of the clustering pattern measured in redshift space compared to the true pat-

tern in real space (see *e.g.* Kaiser 1987). In this section, we analyse the distortions to the shape of the power spectrum measured in redshift space using the N-body simulations described in Section 2. This allows us to quantify the effects of linear and non-linear peculiar velocities and hence to establish the range in wavenumber over which linear perturbation theory can be used to model the distortions. (For a similar analysis of redshift-space distortions in N-body simulations, see Gramman *et al.* 1993). We then compare the redshift-space estimates of  $P(k)$  for the Stromlo-APM survey of the previous section with the real-space estimates of  $P(k)$  for the APM Galaxy Survey derived by Baugh and Efstathiou (1993, hereafter BE) to quantify the effects of redshift-space distortion on large spatial scales.

### 6.1 Redshift-space distortions of $P(k)$ determined from N-body simulations

Figure 9 shows the power-spectra measured in real-space and redshift space for each of the ensembles of N-body simulations described in Section 2. In each case, the amplitude of the power spectrum measured in redshift space is enhanced on large scales compared to the power spectrum measured in real space. In linear perturbation theory, the power spectrum in redshift-space,  $P_s(k)$ , is related to the power-spectrum in real-space,  $P_r(k)$ , according to the formula

$$P_s(\mathbf{k}) = P_r(\mathbf{k}) (1 + \beta\mu^2)^2, \quad \beta = \frac{\Omega^{0.6}}{b}, \quad (18)$$

(Kaiser 1987). In this equation,  $\mu$  is the angle between the vector  $\mathbf{k}$  and the line-of-sight,  $b$  is a linear bias factor relating fluctuations in the galaxy distribution to fluctuations in the mass distribution,  $(\delta\rho/\rho)_{gal} = b(\delta\rho/\rho)_{mass}$ , and we have assumed that power spectrum is determined from a patch of the universe that subtends a small solid angle at the position of the observer. Averaging equation (18) over the angle  $\mu$ , we obtain

$$P_s(k) = P_r(k) \left(1 + \frac{2}{3}\beta + \frac{1}{5}\beta^2\right). \quad (19)$$

Thus the ratio  $P_s(k)/P_r(k)$  depends on the parameter  $\beta = \Omega^{0.6}/b$  in linear perturbation theory<sup>‡</sup>.

On small scales (wavenumbers  $k \gtrsim 0.1h\text{Mpc}^{-1}$ ), the redshift-space power spectra in Figure 9 are suppressed in amplitude compared to the real-space spectra. This is caused by the small-scale peculiar velocities in high density regions that produce so called ‘fingers of God’ in redshift space. The solid lines in Figure 9 show a simple model derived by Peacock and Dodds (1994) that incorporates both the linear theory distortion of equation (18) with a model for the distortions caused by fingers of God. The small scale peculiar velocities are assumed to be uncorrelated in position and drawn from a Gaussian distribution with 1-dimensional dispersion  $\sigma_v$ . The combined effects lead to the following formula relating the angle averaged power spectra in redshift space and real space:

$$P_s(k) = P_r(k) G(\beta, k\sigma_v) \quad (20)$$

where the function  $G$  is given by

$$G(\beta, k\sigma_v) = \frac{\sqrt{\pi} \operatorname{erf}(k\sigma_v)}{8 (k\sigma_v)^5} [3\beta^2 + 4\beta (k\sigma_v)^2 + 4(k\sigma_v)^4] - \frac{\exp(-(k\sigma)^2)}{4(k\sigma)^4} [\beta^2 (3 + 2(k\sigma)^2) + 4\beta (k\sigma)^2]. \quad (21)$$

The solid lines in Figure 9 show equation (20) for each ensemble, where we have used the 1-dimensional velocity dispersion determined from the simulations  $\sigma_v = 670.5, 344.1,$  and  $510.0 \text{ km s}^{-1}$  for the SCDM, LCDM and MDM ensembles respectively. These curves provide a good match to the results from the N-body simulations over the range of wavenumbers plotted in Figure 9 and are more accurate than the model described by Gramman *et al.* (1993). Nevertheless, the model of equation (20) is simplistic, as it ignores non-linear streaming of galaxy pairs (cf. eg. Nusser and Fisher (1995)).

Figure 10 shows the ratio of the power spectra plotted in Figure 9. The solid lines show the linear theory relation of equation (19) and the dotted lines show equation (20). These results show that at wavenumbers  $k \gtrsim 0.1h\text{Mpc}^{-1}$ , small-scale peculiar velocities cause a significant reduction in the amplitude of the power spectrum measured in redshift space. One must therefore be cautious in determining  $\beta$  from redshift distortions using the linear relations equations (18) and (19). The range of validity of linear theory is strongly dependent on the amplitude of the small-scale peculiar velocity field, as expected from equation (20). The biases can be large, for example, even at  $k = 0.1h\text{Mpc}^{-1}$ , the ratio of the power spectra in the MDM model is equal to 1.57 compared to the linear theory prediction of 1.87.

The amplitude of the small-scale peculiar velocity field is relatively poorly constrained by observations. For example, Davis and Peebles (1983) found an *rms* relative peculiar velocity of  $v_{12} = 340 \pm 40\text{kms}^{-1}$  between galaxy pairs separated by  $\sim 1 h^{-1}\text{Mpc}$  from an analysis of the CfA-1 survey and Bean *et al.* 1983 found  $v_{12} = 250 \pm 50\text{kms}^{-1}$  from an analysis of a smaller, but deeper survey. However, values as high as  $600\text{--}800\text{kms}^{-1}$  have been derived in the literature (Hale-Sutton *et al.* 1989, Mo *et al.* 1993). The best constraints on  $v_{12}$  for optical galaxies come from an analysis of the CfA2 and Southern Sky Redshift Survey by Marzke *et al.* (1995) who find  $v_{12} = 540 \pm 180\text{kms}^{-1}$ . The error on  $v_{12}$  is large and the Marzke *et al.* results are consistent with the small-scale peculiar velocities ( $\sigma_v \sim v_{12}/\sqrt{2}$ ) for the mass points in the LCDM and MDM models but are lower than those of COBE normalized SCDM models. In principle, with a larger survey, we could use equations (20) and (21) (or a more complicated non-linear model) to simultaneously determine the parameters  $\beta$  and  $\sigma_v$  (see Cole *et al.* 1995, for an application to redshift surveys of IRAS galaxies).

In addition to the effects of non-linear peculiar velocities, biases in the estimates of  $P(k)$  derived from equation (12) will also introduce departures from the linear theory predictions for the ratio  $P_s(k)/P_r(k)$  at small wavenumbers. This is illustrated in Figure 11, where we have plotted the ratio of the redshift-space power spectra of the mock Stromlo-APM simulations to the real-space power spectra measured from the full N-body simulations. The decline in the ratio at  $k \lesssim 0.05h\text{Mpc}^{-1}$  is caused by the biases in the

<sup>‡</sup> This is true even for low density spatially flat models, see Peebles (1984) and Lahav *et al.* (1991)

power spectrum estimates discussed in Appendix A. Even at wavenumber  $k \sim 0.05 h\text{Mpc}^{-1}$ , the ratios for the LCDM and MDM ensembles fail to reach the linear predictions primarily because the convolution of the redshift space power spectrum with the window function causes a slight depression in its amplitude (*cf* the dotted lines in Figure 3).

## 6.2 Estimates of $\beta$ from redshift space distortion

In this Section, we estimate  $\beta$  by comparing the Stromlo-APM power spectrum with real space estimates of  $P(k)$  for the APM survey. Baugh and Efstathiou (1993) have described a method for recovering the three-dimensional power spectrum from the angular two-point correlation function  $w(\theta)$ . The inversion requires a knowledge of the redshift distribution of the galaxies used to estimate  $w(\theta)$ , of the geometry of the Universe and of the evolution of the power spectrum. The redshift distribution of APM galaxies is well constrained by observations (see Maddox *et al.* 1995). However, BE show that uncertainties in the evolution of  $P(k)$  and the cosmological model introduce uncertainties of  $\sim 20\%$  in the amplitude of the real space power spectrum. As an illustration of these uncertainties, we will use two estimates of the real space power spectrum derived from APM galaxies in the magnitude range  $17 < b_J < 20$  (plotted in Figure 12). In these inversions we assume an Einstein-de Sitter universe and a power spectrum that evolves as  $P(k, z) = P(k)/(1+z)^\alpha$  with  $\alpha = 0$  (filled circles) and  $\alpha = 1.3$  (open circles) corresponding to a clustering pattern that is stable in comoving and physical coordinates respectively (see BE for further details). Uncertainties in the redshift distribution and cosmological model introduce similar systematic differences in the real space power spectra, but since these errors are considerably smaller than the random errors in the redshift space estimates of  $P(k)$ , we will not discuss them in detail here.

The open squares in Figure 12 show the  $z_{max} = 0.06$  redshift-space estimate of  $P(k)$  for the Stromlo-APM survey as calculated in Section 2.2. Qualitatively, the behaviour is similar to that seen in the simulations; at wavenumber  $k \lesssim 0.03 h\text{Mpc}^{-1}$  the redshift-space power spectrum declines and falls below the real space estimates. Over the wavenumber range  $0.03 \lesssim k \lesssim 0.07 h\text{Mpc}^{-1}$  the redshift-space amplitude is enhanced suggesting a significant distortion of the clustering pattern in redshift space. At larger wavenumbers, the errors in the Stromlo-APM power spectrum become large because it is a sparse sampled redshift survey and so contains little information on the small-scale clustering of galaxies.

We estimate the amplitude of the redshift space distortions in the Stromlo-APM survey as follows. We compute the ratio  $P_s(k)/P_r(k)$  by linear interpolating the real-space power spectra plotted in Figure 12 and we average this ratio over the wavenumber range  $0.05 < k < 0.1 h\text{Mpc}^{-1}$ . This leads to an estimate of  $\beta$  from equation 19. To estimate the error in  $\beta$ , we compute the scatter in the ratio of the redshift-space to real-space power-spectra from the mock Stromlo-APM surveys plotted in Figure 11 averaged over the same wavenumber range as the data. This provides an estimate of errors associated with sampling fluctuations in the redshift survey. We estimate the error associated with uncertainties in the real space estimate of  $P(k)$  from the scatter

	$\alpha=0.0$	$\alpha=1.3$
	$\beta$	$\beta$
Flux Weighted $P_s(k)$	$0.74 \pm 0.48$	$0.20 \pm 0.44$
Volume Limited $P_s(k)$	$0.38 \pm 0.67$	$-0.13 \pm 0.64$

**Table 1.** Estimates of  $\beta$  from the Stromlo-APM survey.

in the ratio  $P_s(k)/P_r(k)$  using  $P_r(k)$  determined from four roughly equal area zones of the APM survey (see BE). Our final error estimate on  $\beta$  is derived by adding these two error terms in quadrature on the assumption that they are uncorrelated. Table 1 shows our estimates of  $\beta$  derived using the two real-space estimates of  $P(k)$  plotted in Figure 12, and two estimates of the redshift-space power spectrum for the Stromlo-APM survey; the  $z_{max} = 0.06$  volume limited results plotted in Figure 12 and the flux-limited results from Figure 6, with a weight function (equation 15) in which we have set  $P(k) = 8000(h^{-1}\text{Mpc})^3$ .

These results suggest a positive value of  $\beta$ , though the errors are large. The differences in the flux-weighted and volume limited estimates of  $P(k)$  over the wavenumber range  $0.05 < k < 0.1 h\text{Mpc}^{-1}$  lead to an uncertainty of nearly a factor of two in the derived value of  $\beta$ . A similar uncertainty is introduced by the difference in the real-space estimates of  $P(k)$  derived from the APM survey for the two adopted values of the evolution parameter  $\alpha$ .

The inferred errors on  $\beta$  are larger than those quoted in other analyses of redshift space distortions. For example, Hamilton (1993) finds  $\beta = 0.66^{+0.34}_{-0.22}$  from an analysis of angular moments of the two-point correlation function of the 1.9Jy IRAS redshift survey of Strauss *et al.* (1992); Cole *et al.* (1995) analyse angular harmonics of the power spectrum and find  $\beta = 0.52 \pm 0.13$  and  $\beta = 0.54 \pm 0.3$  for the 1.2Jy and QDOT IRAS surveys respectively. Loveday *et al.* (1995b) find  $\beta = 0.48 \pm 0.12$  from an analysis of anisotropies in the redshift-space correlation function of the Stromlo-APM survey. At face value our estimates of  $\beta$  appear to disagree with those of Loveday *et al.*, who analyse the same survey. However, it seems likely that Loveday *et al.* have underestimated the error on  $\beta$ . As a further check of whether our errors are realistic, Table 2 list the errors and biases in  $\beta$  derived by applying the above analysis to the mock Stromlo-APM surveys constructed from the simulations. Here we have computed  $\beta$  from the ratio of the redshift-space power spectra of the mock surveys to the mean real-space power spectrum for each ensemble, and we have neglected errors in the real-space estimate  $P(k)$  since these are negligible. In each case, the errors in  $\beta$  are close to  $\delta\beta \approx 0.5$  in good agreement with our error estimates for the real data. In addition, Table 2 shows that  $\beta$  is underestimated in each case because of the nonlinear corrections described in the previous subsection and because of the biases in the redshift-space estimates of  $P(k)$  described in Appendix A.

The results given in Table 1 are in good agreement with those determined by Baugh (1995) from a comparison of the redshift-space two-point correlation function of the Stromlo-APM survey and the real-space correlation function inferred by inverting the angular correlation function of the APM survey.

Our analysis suggests that the results of Table 1 should

Model	$\beta$	$\delta\beta$	Linear $\beta$
SCDM	0.64	0.54	1.00
LCDM	0.13	0.55	0.38
MDM	0.62	0.52	1.00

**Table 2.** Estimates of  $\beta$  derived from the ratio  $P_s/P_r$  over the wavenumber range  $0.05 < k < 0.1 h\text{Mpc}^{-1}$  from mock Stromlo-APM surveys.

be considered as lower bounds on the true value of  $\beta$  and hence that  $\beta = 1$  is compatible with the observations. With larger redshift surveys it should be possible to fit a more complicated model to the data so extending the useable range of wavenumbers and reducing the biases in  $\beta$ , *e.g.* equation 21 with  $\beta$  and  $\sigma_v$  as free parameters, or the non-linear model of Nusser and Fisher (1995) based on the Zel-dovich approximation.

## 7 CONCLUSIONS

The conclusions of this paper are as follows:

[1] We have tested estimators of  $P(k)$  using simulated redshift surveys constructed from N-body simulations. These tests show that estimates of  $P(k)$  are biased at low wavenumbers if the surveys are used to estimate the mean galaxy density. Formulae for these biases are given in Appendix A.

[2] We have estimated  $P(k)$  for the Stromlo-APM redshift survey using volume limited and flux limited samples. The power spectra are insensitive to the volume limit and to the galaxy weights applied in the analysis of flux limited samples.

[3] We have investigated whether the amplitude of  $P(k)$  depends on galaxy luminosity and used N-body simulations to assess the statistical significance of our analysis. We find no evidence for any significant luminosity dependence except possibly at absolute magnitudes brighter than  $M = -20.3$ , where we find some evidence for a higher amplitude. This is broadly consistent with the analysis of the CfA-2 redshift survey by Park *et al.* (1994) who find that the amplitude of  $P(k)$  for galaxies brighter than  $M^*$  is about 40% higher than the amplitude measured from fainter galaxies.

[4] We have analysed numerical simulations to determine the effects of redshift-space distortions on the shape of  $P(k)$ . The distortions can be well approximated by the formula of Peacock and Dodds (1994), equation (20), which depends on two parameters,  $\beta = \Omega^{0.6}/b$  and a measure of the small-scale rms peculiar velocity,  $\sigma_v$ .

[5] We estimate the redshift-space distortions in the Stromlo-APM survey by comparing redshift-space power spectra with estimates of the real-space power spectrum determined by inverting the angular correlation function measured for the parent APM Galaxy Survey. The results indicate a positive value of  $\beta$ , consistent with other work, but the uncertainties are large and do not exclude  $\beta = 1$ .

In Figure 13, we compare the Stromlo-APM power spectrum with power spectra estimated from other surveys. The filled circles show the flux limited estimates of  $P(k)$  for the Stromlo-APM survey using  $P(k) = 8000 (h^{-1}\text{Mpc})^3$

in the weighting scheme of equation (15). The open symbols show  $P(k)$  for the combined 1.2Jy and QDOT IRAS redshift surveys, as analysed by Tadros and Efstathiou (1995); these estimates are for a flux limited sample with  $P(k) = 8000 (h^{-1}\text{Mpc})^3$  in the weighting scheme of equation (15). The filled stars show  $P(k)$  from Park *et al.* (1994) for a volume limited subset of the CfA-2 survey consisting of 1509 galaxies to a coordinate distance of  $101h^{-1}\text{Mpc}$ . The power spectra for the two optically selected catalogues are consistent with each other within the errors, but the amplitude of the IRAS power spectrum is slightly lower indicating that IRAS galaxies are less strongly clustered than optically selected galaxies. The results shown in Figure 13 are consistent with a linear relative bias between optical and IRAS galaxies of  $b_{opt}/b_{IRAS} \sim 1.2$ . Recently, Landy *et al.* (1996) have computed a 2 dimensional power spectrum for the Las Campanas redshift survey and find evidence for a strong peak in the power spectrum at wavenumbers  $k \sim 0.06h\text{Mpc}^{-1}$ . Their results are not easily comparable to ours and it is unclear whether there is any inconsistency with the three dimensional power spectrum inferred for the APM Galaxy survey (Baugh and Efstathiou 1993) or with the redshift space power spectrum of the Stromlo-APM survey presented here. A detailed comparison is deferred to a subsequent paper.

In Figure 13b, we show the empirical estimates of  $P(k)$  together with redshift-space estimates of  $P(k)$  determined from N-body simulations of the LCDM, MDM, and SCDM models. The shape of the SCM curve is in good agreement with the power spectra measured for the IRAS and CfA-2 surveys, though it lies low compared to the Stromlo-APM data points at wavenumber  $k \sim 0.05h\text{Mpc}^{-1}$ . The high amplitude for the SCDM model implied by the COBE temperature anisotropies results in a high amplitude for the peculiar velocity field. This in turn leads to a significant difference in the shape of the redshift-space power spectrum compared to the real-space power spectrum (see also Bahcall *et al.* 1993) and so the model can provide an acceptable match to the redshift-space  $P(k)$  although it fails to match the shape of the real-space power spectrum (see *e.g.* BE, Maddox *et al.* 1995). As mentioned in Section 6.1, the small scale ( $\sim 1h^{-1}\text{Mpc}$ ) relative peculiar velocities predicted by the COBE normalised SCDM model are considerably higher than the relative motions between galaxy pairs measured by Marzke *et al.* (1995). Both the LCDM and MDM models provide acceptable fits to the power spectra measured from the redshift surveys and distinguishing between these models would require accurate estimates of the effects of redshift space distortions. As we have seen from the analysis of the Stromlo-APM survey, larger redshift surveys, such as the AAT 2-degree field redshift survey (see Efstathiou 1996) and the Sloan Digital Sky Survey (Gunn & Weinberg 1995) are required to determine  $\beta$  accurately and so distinguish between these models.

## ACKNOWLEDGMENT

HT and GPE acknowledge the receipt of a PPARC studentship and Senior Fellowship respectively. We thank Carlton Baugh and Jon Loveday for useful conversations and for comments on the manuscripts. We thank Jon Loveday,

Bruce Peterson and Steve Maddox for their invaluable contributions to the Stromlo-APM redshift survey.

## References

- Bahcall N. A., Cen R. & Gramman M., 1993, *ApJ* **408**, L77  
 Baugh C.M. & Efstathiou G., 1993, *MNRAS*, **265**, 145.  
 Baugh C.M. & Efstathiou G., 1994, *MNRAS*, **267**, 323.  
 Baugh C. M., 1995 *in preparation*  
 Baumgart D. J. & Fry J. N., 1991, *ApJ*, **375**, 25  
 Bean A. J., Efstathiou G., Ellis R. S., Peterson B. A. & Shanks T., 1983, *MNRAS*, **205**, 605  
 Bond J. R. & Efstathiou G., 1984, *ApJ*, **285** L45  
 Cole S., Fisher K. B. & Weinberg D. H., 1995, *MNRAS*, **275**, 515  
 Croft R. A. C., & Efstathiou G., 1994, *MNRAS*, **268**, L23  
 Davis M. & Peebles P. J. E., 1983 *Apj*, bf 267, 465  
 Davis M., Efstathiou G., Frenk C. S. & White S. D. M., 1985, *ApJ*, **292**, 371  
 Efstathiou G., Davis M., Frenk C. S. & White S. D. M., 1985, *ApJS*, **57**, 241  
 Efstathiou G., Ellis R. S. & Peterson B. A., 1988, *MNRAS*, **232**, 431  
 Efstathiou G., 1996, ‘*Observations of Large-Scale Structure in the Universe*’, Les Houches Lectures 1995, ed R. Schaeffer, Elsevier Science Publishers, Netherlands, in press.  
 Feldman H.A., Kaiser N. & Peacock J.A., 1994, *ApJ*, **426**, 23.  
 Fisher K.B., Davis M., Strauss M.A., Yahil A. & Huchra J.P., 1993, *ApJ*, **402**, 42.  
 Gramman M., Cen R. & Bahcall N. A., 1993, *ApJ*, **419**, 440  
 Gunn J. E. & Weinberg D. H., 1995, ‘*Wide Field Spectroscopy and the Distant Universe, The 35<sup>th</sup> Herstmonceux Conference*’ eds. S. J. Maddox & A. Aragon-Salamanca  
 Hale-Sutton D., Fong R., Metcalfe N. & Shanks T., 1989, *MNRAS*, **237**, 569  
 Hamilton A. J. S., 1988, *ApJ*, **331**, L59  
 Hamilton A. J. S., 1993, *ApJ*, **406**, L47  
 Iovino A., Giovanelli R., Haynes M., Chincarini G. & Guzzo L., 1993, *MNRAS*, **265**, 21  
 Kaiser N., 1987, *MNRAS*, **227**, 1  
 Klypin A., Holtzman J., Primack J. & Regos E., 1993, *ApJ*, **416**, 1  
 Lahav O., Lilje P. B., Primack J. R. & Rees M., *MNRAS* 1991, **251**, 128  
 Landy S. D., Schectman S. A., Lin H., Kirshner R. P., Oemler A. A. & Tucker D., 1996 *preprint*  
 Loveday J., Efstathiou G., Peterson B. A. & Maddox S. J., 1992a, *ApJ*, **400**, L43  
 Loveday J., Peterson B. A., Efstathiou G. & Maddox S. J., 1992b, *ApJ*, **390**, 338  
 Loveday J., Maddox S. J., Efstathiou G. & Peterson B. A., 1995a, *ApJ*, **442**, 457  
 Loveday J., Efstathiou G., Maddox S. J. & Peterson B. A., 1995b *preprint*  
 Maddox S. J., Sutherland W. J., Efstathiou G. & Loveday J., 1990a, *MNRAS* **243**, 692  
 Maddox S. J., Efstathiou G. & Sutherland W. J., 1990b, *MNRAS*, **246**, 433  
 Maddox S. J., Efstathiou G. & Sutherland W. J., 1995 *submitted*  
 Marzke R. O., Geller M. J., da Costa L. N. & Huchra J. P., 1995 *preprint*  
 Mo H. J., Jing Y. P. & Börner G., 1993, *MNRAS*, **264**, 825  
 Nusser A. & Fisher K. B., 1995 *preprint* astro-ph/9510049  
 Park C., Gott J. R. & da Costa L. N., 1992, *ApJL*, **392**, L51  
 Park C., Vogeley M. S., Geller M. J., & Huchra J. P., 1994 *ApJ*, **431**, 569  
 Peacock J. A. & Dodds S. J., 1994, *MNRAS*, 267, 1020  
 Peebles P. J. E., 1984 *ApJ*, **284**, 439  
 Santiago B. X. & da Costa L. N., 1990, *ApJ*, **362**, 386  
 Schechter P. L., 1976, *ApJ*, **203**, 297  
 Smoot G. F. *et al.* 1992, *ApJ*, **396**, L1  
 Strauss M. A., Huchra J. P., Davis M., Yahil A., Fisher K. B. & Tonry J., 1992, *ApJS*, **83**, 29  
 Tadros H. & Efstathiou G., 1995, *MNRAS*, **276**, L45  
 Vogeley M. S., Park C., Geller M. J. & Huchra J. P., 1992, *ApJ*, **391** L5

Appendix A: Biases in estimating  $P(k)$ 

The quantity  $\Delta(k)$  defined in equation (10) requires an estimate of the mean galaxy density  $\bar{n}$ . Usually, this estimate will be derived from the sample itself, *e.g.* for a volume limited sample we can estimate  $\bar{n}$  from

$$\bar{n} = \frac{1}{V_s} \sum_i n_i W(\mathbf{x}_i) \quad (A1)$$

where  $V_s$  is the volume of the survey and the sum extends over all infinitesimal cells of galaxy count  $n_i$ . Inserting (A1) into equation (10), we find that the expectation value of  $|\Delta(k)|^2$  is given by,

$$\begin{aligned} \langle |\Delta(\mathbf{k})|^2 \rangle &= \frac{\bar{n}}{V} \sum_{\mathbf{k}'} |\hat{W}(\mathbf{k}')|^2 + \frac{\bar{n}^2}{V} \sum_{\mathbf{k}'} |\hat{W}(\mathbf{k} - \mathbf{k}')|^2 P(\mathbf{k}') \\ &- \frac{\bar{n}}{V_s} |\hat{W}(\mathbf{k}')|^2 + \frac{\bar{n}^2}{V_s^2} \int \int \xi(x_{12}) W(\mathbf{x}_1) W(\mathbf{x}_2) |\hat{W}(\mathbf{k}')|^2 dV_1 dV_2 \\ &- \frac{\bar{n}^2}{VV_s} \int \int \xi(x_{12}) W(\mathbf{x}_1) W(\mathbf{x}_2) \hat{W}(\mathbf{k}') e^{i\mathbf{k} \cdot \mathbf{x}_1} dV_1 dV_2 \\ &- \frac{\bar{n}^2}{VV_s} \int \int \xi(x_{12}) W(\mathbf{x}_1) W(\mathbf{x}_2) \hat{W}(\mathbf{k}')^* e^{-i\mathbf{k} \cdot \mathbf{x}_2} dV_1 dV_2 \quad (A2) \end{aligned}$$

The last four terms in equation (A2) account for the biases in estimating  $P(k)$  when the mean galaxy density is determined from the sample itself. The first double integral in equation (A2) measures the excess variance in the galaxy fluctuations above Poisson noise averaged over the survey volume,

$$\sigma_s^2 = \frac{1}{V_s^2} \int \int \xi(x_{12}) W(\mathbf{x}_1) W(\mathbf{x}_2) dV_1 dV_2. \quad (A3)$$

If this variance is dominated by fluctuations on scales smaller than the scale of the survey, it is a good approximation to set the other two integrals in (A2) equal to equation (A3). An approximate expression for the bias in  $|\Delta(k)|^2$  is therefore,

$$\begin{aligned} &- \frac{\bar{n}}{V_s} |\hat{W}(\mathbf{k}')|^2 - \bar{n}^2 \sigma_s^2 |\hat{W}(\mathbf{k}')|^2 \quad (A4.1) \\ &\equiv - \frac{\bar{n}}{V_s} |\hat{W}(\mathbf{k}')|^2 - \bar{n}^2 \left( \sum_{\mathbf{k}'} |W(\mathbf{k}')|^2 P(\mathbf{k}') \right) |\hat{W}(\mathbf{k}')|^2 \quad (A4.2) \end{aligned}$$

where in (A4.2) we have written  $\sigma_s^2$  in terms of the power spectrum  $P(k)$ . We have used these equations to compute the dashed lines shown in Figure 3 in Section 4.2. The first term in each of equations (A4.1) and (A4.2) introduces a bias in the estimate of  $P(k)$  (equation 12) that depends on the number of galaxies in the survey, but is independent of the shape of the power spectrum; the second term introduces a bias that is independent of the number of galaxies in the sample, but depends on the shape of the power spectrum.

It is straightforward to generalise this analysis to the FKP estimator of  $P(k)$  for flux limited samples. As discussed in Section 3.1, we estimate the mean galaxy density by computing the sum

$$\frac{1}{V_{eff}} \sum_i n_i w'(x_i) W(\mathbf{x}_i) \quad (A5.1)$$

where

$$V_{eff} = \int w'(x_i) W(\mathbf{x}_i) dV \quad (A5.2)$$

and the weight function  $w'(x)$  is equal to

$$w' = \frac{1}{(1 + 4\pi\bar{n}(x)J_3)}. \quad (A5.3)$$

Inserting this expression into equation (2.1.4) of FKP, we can calculate the bias in a similar way to the calculation of equation A2. As the final expression is lengthy, we do not reproduce it here.

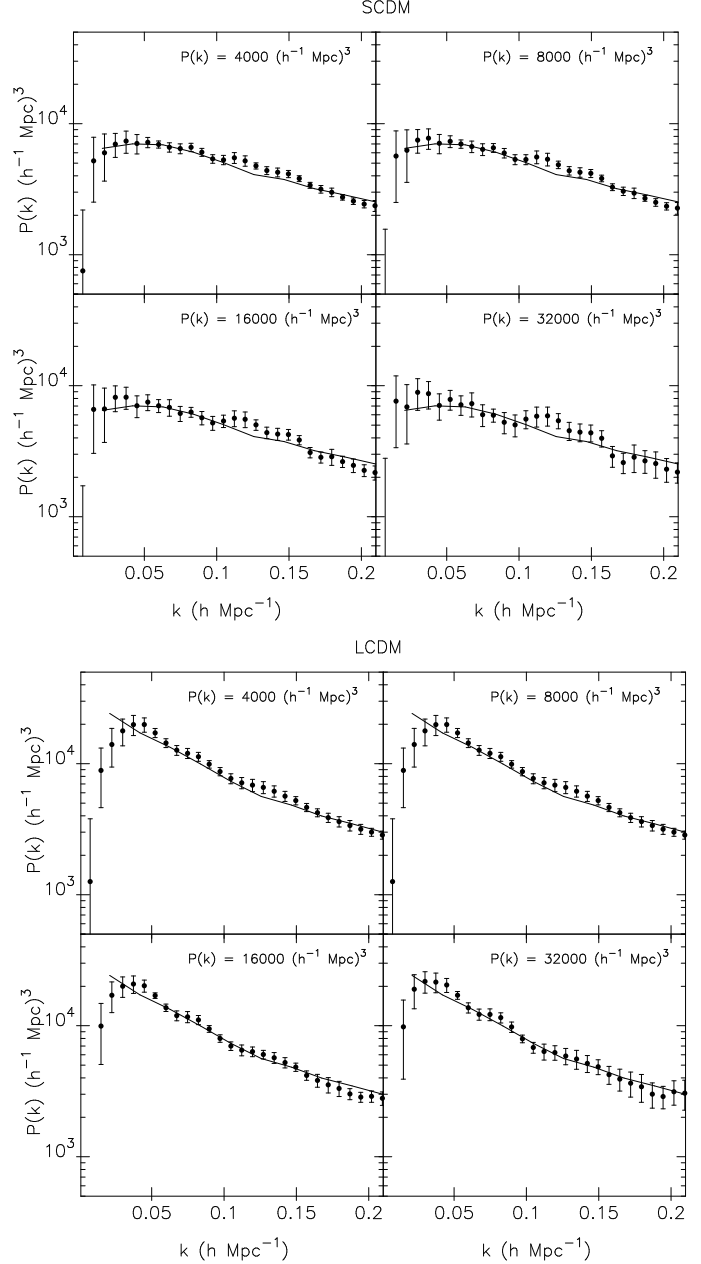


**Figure 4.** Flux weighted power spectra determined from mock sparsely sampled Stromlo-APM surveys. The upper figure shows results for the SCDM ensemble and the lower figure shows results for the LCDM ensemble. The solid line in each panel shows the mean power spectrum determined from the full N-body simulations, as plotted in Figure 3. The points show the average over ten mock Stromlo-APM surveys for four values of  $P(k)$  in the weighting scheme of equation (15),  $P(k) = 4000, 8000, 16000, 32000(h^{-3}\text{Mpc})^3$ , as indicated in each panel. The error bars show one standard deviation on the mean.

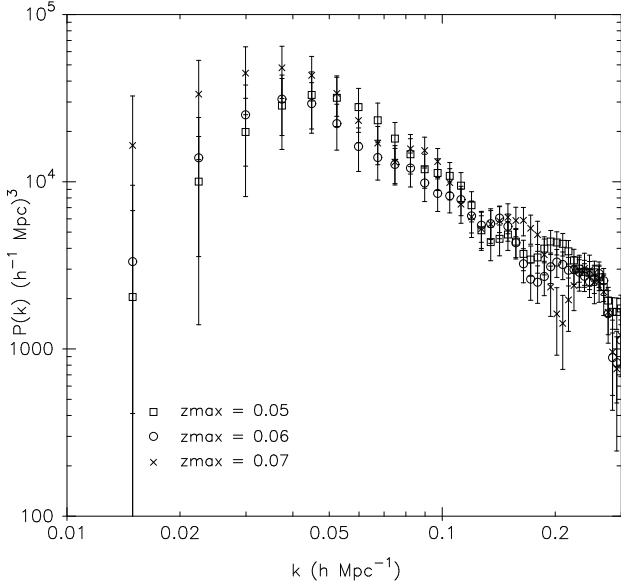


**Figure 5.** Volume limited power spectra of the Stromlo-APM survey, volume limited at  $z = 0.05, 0.06, 0.07$  ( $150 h^{-1}\text{Mpc}$ ,  $180 h^{-1}\text{Mpc}$ , and  $210 h^{-1}\text{Mpc}$ ).

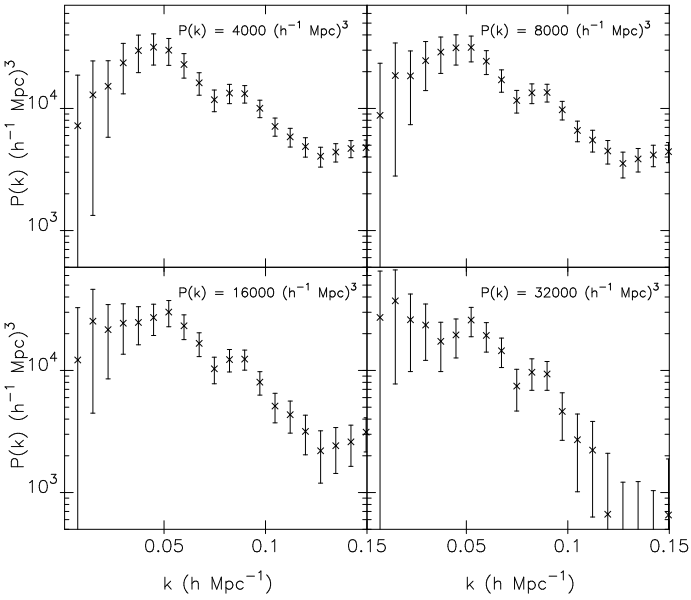


**Figure 6.** Flux limited power spectra of the Stromlo-APM survey for four values of  $P(k)$  in the weighting scheme of equation 15,  $P(k) = 4000, 8000, 16000, \text{ and } 32000(h^{-3}\text{Mpc})^3$  as indicated in each panel.

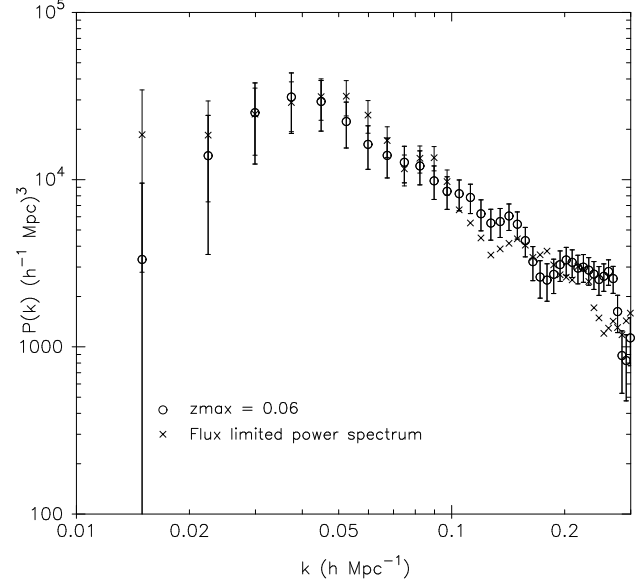


**Figure 7.** Comparison of the volume and flux limited power spectra estimated from the Stromlo-APM survey. The circles show the volume limited power spectrum for the  $z_{max} = 0.06$  sample as plotted in Figure 5 and the crosses show the flux limited power spectrum with  $P(k) = 8000(h^{-3}\text{Mpc})^3$  in equation (15) as plotted in Figure 6. We plot  $1\sigma$  error bars, but we have suppressed the errors on the flux limited estimates at high wavenumbers for clarity.

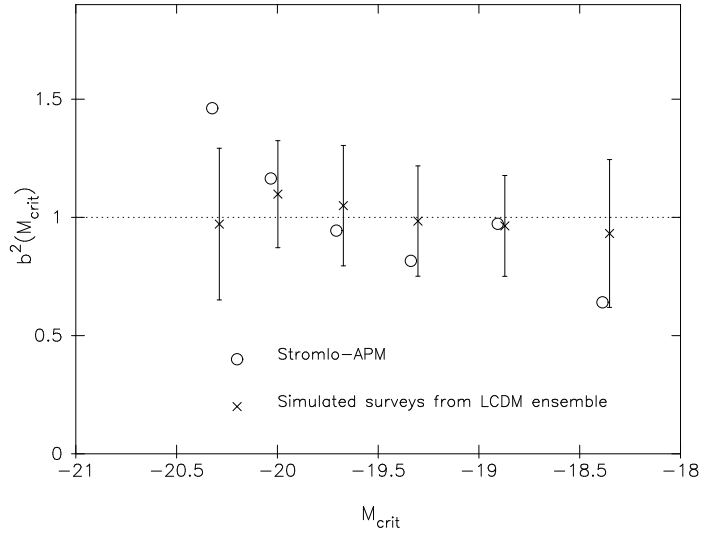


**Figure 8.** The relative bias factor  $b^2$  defined in the text plotted against limiting absolute magnitude  $M_{crit}$ . Circles show the result for the Stromlo-APM data, crosses show the results for simulated Stromlo-APM surveys drawn from the LCDM ensemble. The error bars on these points show the standard deviation of one simulation.

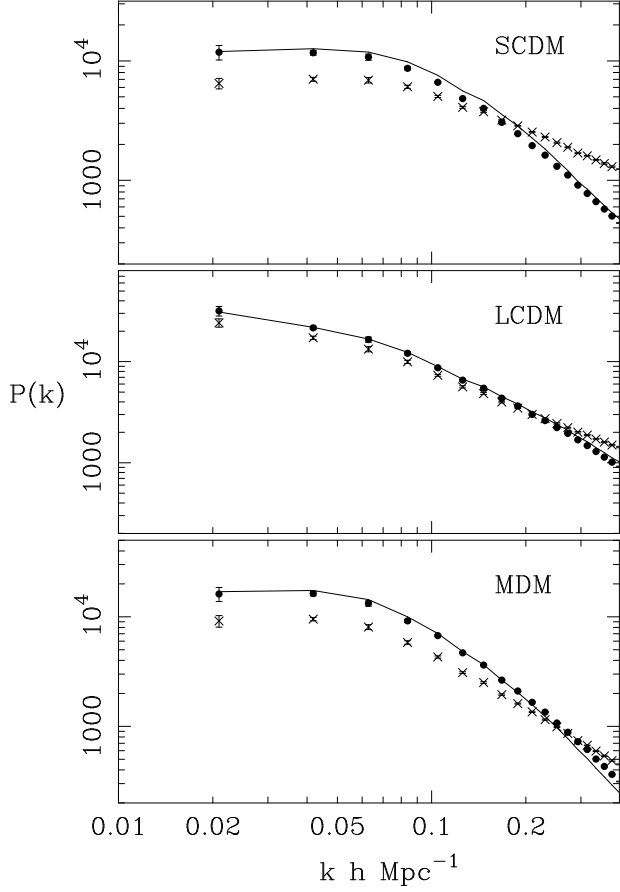


**Figure 9.** Power spectra evaluated in real and redshift space for each ensemble. Redshift space power spectra are shown by the circles and real space spectra are shown by the crosses. The solid lines show the predicted redshift space power spectrum using equation 20 and the measured real space power spectrum. Values for  $\sigma_v$  are given in the text.

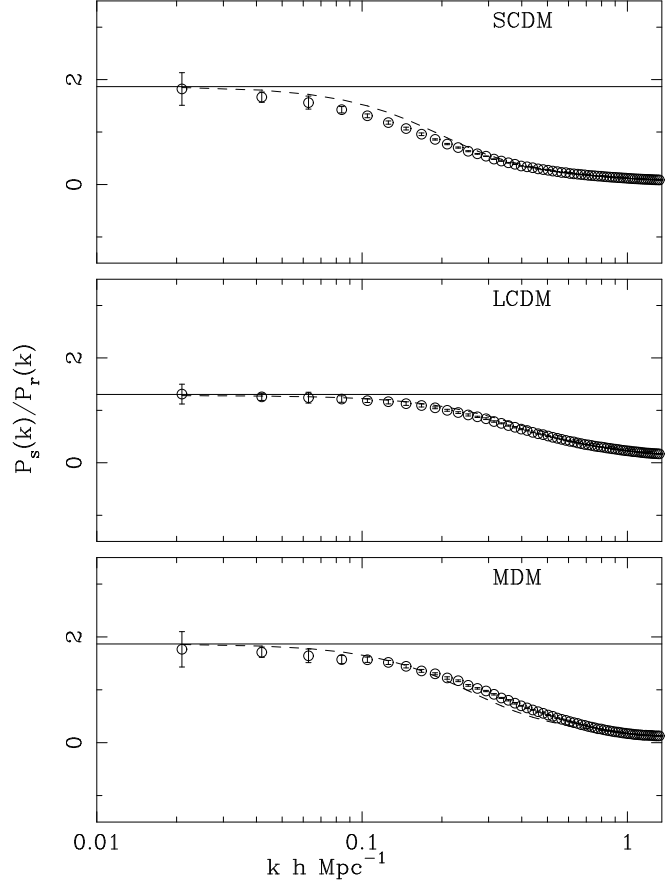


**Figure 10.** The ratio of redshift-space to real-space power for the full N-body simulations (box size  $300 \text{ h}^{-1} \text{ Mpc}$ ). The solid lines shows the linear theory predictions and the dashed lines show equation (20) using the same values of  $\sigma_v$  as in Figure 9.

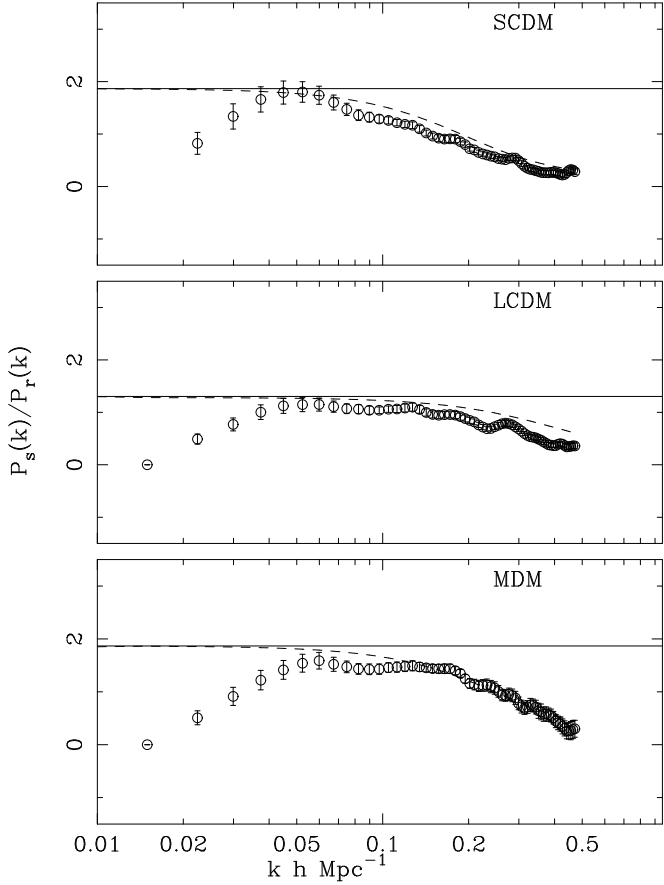


**Figure 11.** The ratios of redshift-space power spectra measured for sparsely sampled mock Stromlo-APM surveys to the real-space power spectra for the full N-body simulations. The solid and dashed lines are as in Figure 10.

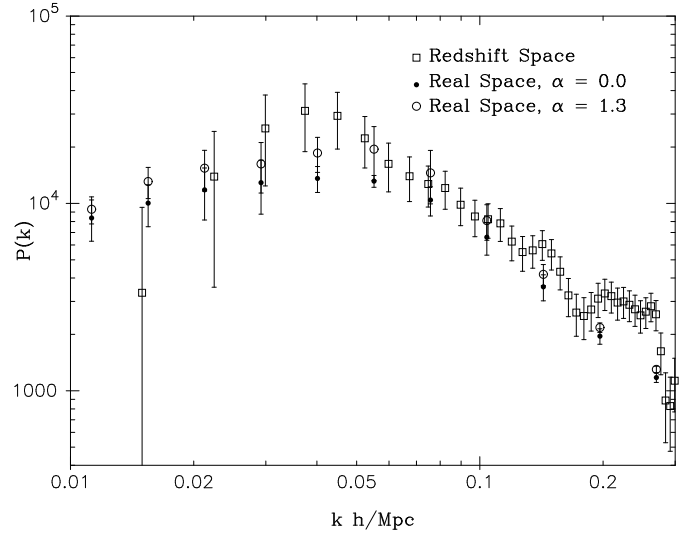


**Figure 12.** The open squares show the redshift-space power spectrum for a volume limited sample from the Stromlo-APM survey limited at  $z_{max} = 0.06$ . The circles show real space power spectra determined using the methods of BE to invert the angular correlation function of APM galaxies in the magnitude slice  $17 < b_J < 20$ . The filled and open circles show the inversion assuming  $\alpha = 0$  and  $\alpha = 1.3$  respectively, where the power spectrum is assumed to evolve according to  $P(k, z) = P(k)/(1+z)^\alpha$ . We have plotted  $1\sigma$  errors on the Stromlo-APM estimates, as in Figure 7. The error bars on the real space power spectra show the standard deviation determined from the scatter in the estimates derived from 4 roughly equal area zones of the APM survey as discussed in BE.

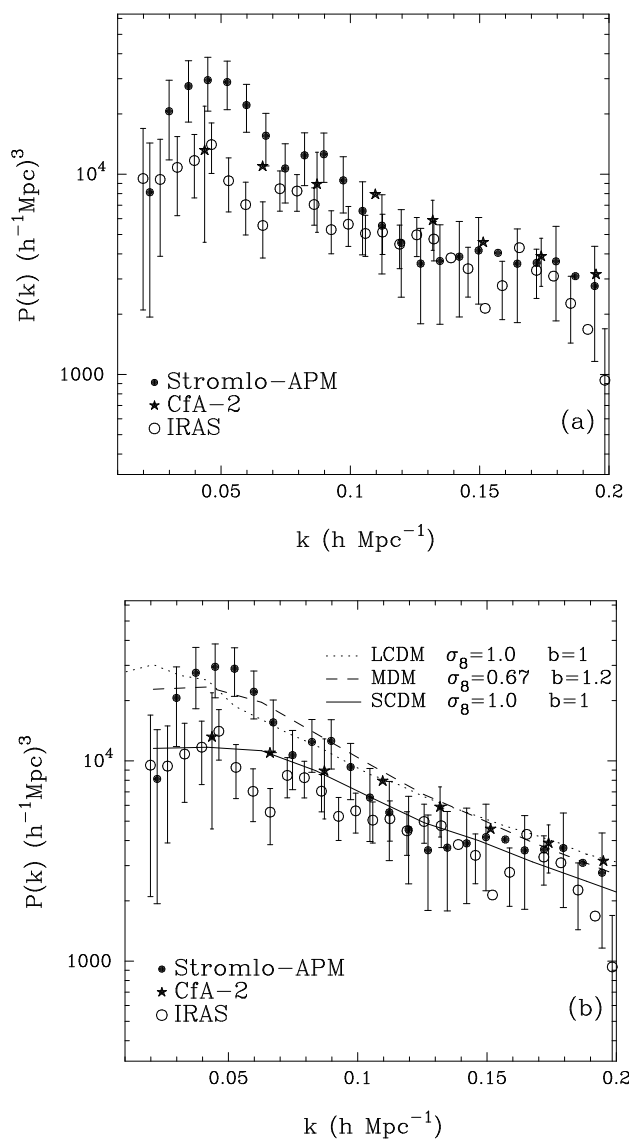


**Figure 13.** Estimates of the power spectra for various redshift surveys. The filled circles show our flux-limited estimates of  $P(k)$  for the Stromlo-APM survey, as plotted in Figure 7. The open circles show a flux limited estimate of  $P(k)$  for IRAS galaxies from Tadros and Efstathiou (1995). The filled stars show estimates of  $P(k)$  from Park *et al.* (1994) for a volume limited subset of the CfA-2 survey. The three curves in Figure (13b) show redshift space power spectra determined from the mass distributions in N-body simulations of the three CDM-like models described in the text;  $\sigma_8$  gives the *rms* amplitude of the mass fluctuations in spheres of radius  $8h^{-1}\text{Mpc}$  and we have multiplied the power spectrum of the MDM model by  $b^2 = (1.2)^2$  to approximately match the power-spectra of the Stromlo-APM and CfA-2 surveys.